Oligodendrocyte precursor cells establish regulatory contacts with the soma of active neurons

Friederike Pfeiffer[1,2]*, Linda L. Boshans[1], Peter Jukkola[1], Madison Beebe[1], Yetunde Akinlaja[1], Ece Begüm Aksoy[2], Ying Sun[2], Constanza Bravo Rossainz Baez[2], Ulrike B. S. Hedrich[3], Ulises Arbelo[1], Akiko Nishiyama[1]

Affiliations:
[1]Department of Physiology and Neurobiology, University of Connecticut, Storrs, USA
[2]Department of Neurophysiology, Institute of Physiology, University of Tübingen, Germany
[3] Department of Neurology and Epileptology, Hertie Institute for Clinical Brain Research, Tübingen, Germany

* To whom correspondence should be addressed.
Friederike Pfeiffer
Address
Department of Neurophysiology,
University of Tübingen
Keplerstr. 15
72074 Tübingen
friederike.pfeiffer@uni-tuebingen.de

ABSTRACT

Oligodendrocyte precursor cells (OPCs) can generate myelinating oligodendrocytes life-long, a process that is dependent on neuronal activity. However, it is possible that OPCs have additional functions, influencing neuronal functions directly. We have used a mouse genetic model of juvenile seizures and chemical induction of neuronal activity to examine the morphological and molecular changes in OPCs around activated principal neurons. We found an increase in process extension of OPCs specifically toward the soma of activated neurons. Moreover, we found that the close proximity of OPC processes around neurons expressing the immediate early gene c-Fos decreased the calcium transients in these neurons, indicating a regulative function of OPCs. Analyses of transcriptome and chromatin accessibility revealed significant changes in genes involved in transforming growth factor beta (TGFβ) signaling. Extracellular matrix genes, particularly those encoding type VI collagen, an established binding partner for the OPC surface protein NG2, was increased around active neurons. Our findings indicate that OPCs are an integral part of the neural network and may help to decrease the activity of neurons that have previously been over-excited, in order to protect these neurons.

Keywords: oligodendrocyte, NG2, VI collagen, extracellular matrix, TGF-β, neuronal activity, c-Fos, RNA-seq, ATAC-seq

INTRODUCTION

Oligodendrocyte precursor cells (OPCs, NG2 glia) are committed to the oligodendrocyte (OL) lineage in the postnatal central nervous system (CNS) (Nishiyama et al., 2021). They are distributed uniformly across the neocortex, in contrast to the distribution of myelinating oligodendrocytes (OLs), which are more abundant in deeper layers, correlating with myelin density (Tomassy et al., 2014). Recent studies have shown that OPCs remodel growing axons (Xiao et al., 2022) and synapses (Auguste et al., 2022; Buchanan et al., 2022). These observations corroborate the notion that OPCs are involved in modulating neuronal function independently of their ability to generate myelinating OLs.

OPCs receive synaptic inputs from neurons (Bergles & Richardson, 2015; Habermacher et al., 2019; Sun et al., 2016). They proliferate in response to acute increase in neuronal firing (Gibson et al., 2014; Li et al., 2010; Oishi et al., 2023; Wennstrom et al., 2003) or differentiate into myelinating oligodendrocytes after sustained or chronically elevated neuronal activity (Chapman et al., 2023; Malone et al., 2013; Nagy et al., 2017; Ortiz et al., 2019; Thornton & Hughes, 2020). However, it is not clear how changes in neuronal activity are detected in OPCs and initiate a signaling pathway that ultimately alters their behavior.

In white matter, OPCs have numerous cell processes, which contact neurons at discrete locations such as the nodes of Ranvier (Butt et al., 1999; Serwanski et al., 2017) where they can sense changes in neuronal firing. Here we explored the spatial relation between OPC processes and neuronal subdomains in gray matter. To examine how OPCs respond to elevated neuronal activity, we used a genetic juvenile seizure model (Dravet et al., 2011) and models of chemogenetic neuronal activation in adult mice and show that OPC processes were more closely apposed to activated c-Fos+ neurons in the hippocampus. Furthermore, calcium dynamics in acute slices showed a more dampened response in those surrounded by OPCs, suggesting a suppressive effect of OPCs on neuronal excitability. Transcriptomic analysis revealed an increase in the expression of extracellular matrix molecules, in particular collagen VI, a known binding partner of NG2.

Our results suggest that OPCs are substantially involved in regulating the activity of the neural network, presumably exerted by approaching (over-)active neurons with their processes, and that their interaction with distinct neuronal subdomains is crucial to exert this regularly and potentially neuroprotective function.

RESULTS

OPC processes are in close proximity to neuronal subdomains in gray matter

In the hippocampal CA1 region, somata of pyramidal neurons are localized in the stratum pyramidale and extend their basal and apical dendrites in strata oriens and radiatum, respectively. PDGFRα immunolabeling of a postnatal day 14 (P14) hippocampus showed OPCs in strata oriens and radiatum, with some located at the border and occasionally within the pyramidal layer (Fig. 1a). The highly branched processes of OPCs covered the neuropil, and some extended across the stratum pyramidale (Fig. 1b), where they surrounded the somata of pyramidal neurons immunolabeled for microtubule-associated protein 2 (MAP-2) (Fig. 1c,d). Other OPC processes were found intertwined with MAP-2+ apical and basal dendrites of neurons (Fig. 1c, e-f). OPC processes were also seen to extend around the axon initial segment (AIS) identified by βIV-spectrin (Fig. 1g).

In the adult hippocampus, OPC processes were also seen in close proximity to the soma and dendrites of biocytin-filled CA1 pyramidal neurons. (Fig. 1h). As in the juvenile hippocampus, OPC processes in the adult hippocampus were found apposed to multiple sites on the neuronal soma labeled for Kv1.2 (Fig. 1i). In addition, multiple processes from single OPCs extended toward and encircled β4-spectrin+ axon initial segments of multiple pyramidal neurons (Fig. 1j). Super-resolution imaging using STED microscopy revealed OPC processes closely apposed to and intwined around the axon initial segment with the banded appearance of βIV-spectrin (Fig. 1k).

Quantification revealed that the length of the axon initial segment contacted by OPC processes was similar to or greater than that contacted by microglia, previously known to contact the axon initial segment (Baalman et al., 2015) (Extended Data Fig. 1).

Active neurons are increasingly surrounded by OPC processes in the juvenile hippocampus

To examine whether the spatial relationship between OPCs and neuronal somata was affected upon an increase in neuronal activity, we used *Vgat*$^{cre/+}$;*Scn1a*$^{A1783V/+}$ mice (Scn1a mutant) as a model of juvenile seizure. The Scn1a mutant mice express the loss-of-function Scn1a-A1783V mutation encoding the voltage-dependent Nav1.1 sodium channel conditionally in GABAergic inhibitory interneurons (Fig. 2a) (Kuo et al., 2019; Ricobaraza et al., 2019), leading to hyperactivity of principal neurons due to reduced inhibitory input. We used littermates *Vgat*$^{cre/+}$;*Scn1a*$^{+/+}$ as control (Scn1a

control). In the Scn1a mutant mice used in this study, there is a cre-dependent missense mutation C5348T in exon 26 of the *Scn1a* gene, which encodes the A1783V variant in the S6 transmembrane region of domain IV of the alpha subunit of voltage-dependent Na^+ channel (Jackson Laboratory, #026133), and mutated gene is expressed specifically in GABAergic neurons (Kuo et al., 2019).

The mutant mice developed normally during the first two weeks after birth. At postnatal day 14 (P14) occasional seizures started to appear, and the mice died after P15, as previously described (Kuo et al., 2019, Ricobaraza et al., 2019). We used P14-15 mutant mice to look for early changes in OPCs after onset of principal neuronal hyperexcitability.

There was no difference in the density of PDGFRα-immunoreactive OPCs in Scn1a control and mutant CA1 (Extended Data Fig 2 a-c). To determine whether overall OPC morphology changed in Scn1a mutant mice, we performed 3D Sholl analysis in the hippocampal CA1 region of Scn1a control and Scn1a mutant mice, using the filament tool in Imaris (Extended Data Fig. 3a). In the stratum oriens, OPCs in the mutant had significantly more intersections at 18-21, 23 and 27µm away from the OPC center (Extended Data Fig. 3b), suggesting greater complexity of distal OPC processes in the stratum oriens. There were no significant differences when comparing OPCs from mutant or control mice in the stratum radiatum (Extended Data Fig. 3c) or the stratum pyramidale (Extended Data Fig. 3d).

We next determined whether OPC processes were more prevalent around active neurons that expressed the immediate early gene product c-Fos (Greenberg & Ziff, 1984; Milbrandt, 1986), which is upregulated in a variety of seizure states (Morgan & Curran, 1989). *Fos* transcriptional activity has been used as an indicator of actively firing neurons (Barth et al., 2004). In both control and mutant mice, we found c-Fos positive neurons to be surrounded by PDGFRα-positive OPC processes (Fig 2b-e). We performed Sholl analysis by positioning the starting point for automated filament reconstruction in Imaris onto either c-Fos-positive, or c-Fos-negative neuronal soma in CA1 stratum pyramidale and assessed the number of neurons that were surrounded by 5-10 OPC processes within 10-µm distance around the soma center of the neuron (Fig. 2f). In Scn1a control mice, there were 2.3-fold more c-Fos-positive neurons that were contacted by 5-10 OPC processes emanating from a nearby OPCs within a 10µm radius compared to c-Fos-negative neurons. Similarly, in Scn1a mutant CA1, 1.8-fold more c-Fos-positive neurons were contacted by OPC processes than c-Fos-negative neurons. There was no significant difference in the number of neurons with 5-10 OPC processes around c-Fos-positive neurons between control and mutant mice, nor was there a significant difference between c-Fos-negative neurons. Thus, regardless of the

Scn1a genotype, OPC processes preferentially encircled nearby c-Fos-positive active neurons, suggesting that the increase in physiological levels of individual neuronal activity is a key determinant for attracting OPC processes towards them.

OPC processes surround chemogenetically activated neurons in adult hippocampus

To examine whether the dynamic changes in OPC processes were a unique property of OPCs responding to active neurons in the juvenile hippocampus of Scn1a mutants or a more general phenomenon that also occurred in older mice, we used a chemogenetic approach to activate Ca^{2+} signal in pyramidal neurons in adult mice. In Camk2a-cre (T29-1) tg/+; CAG-LSL-Gq-DREADD (CAG-CHRM3-mCitrine) tg/+ double transgenic mice, Gq-DREADD is expressed in pyramidal neurons. We injected 100 µg /kg deschloroclozapine (dcz) or vehicle and harvested the brains after 6 hours. In dcz-injected mice, c-Fos expression was prominently elevated in CA1 compared with c-Fos in vehicle-injected mice (Figure 3 a and b), and c-Fos immunoreactivity was stronger than that in CA2/3 (boxes in Figure 3 a and b).

We examined whether there was a difference in the distance between the soma of an OPC and an adjacent pyramidal neuron (scheme in Fig. 3c). In Imaris, we used machine learning to train the software to detect c-Fos+ neurons (Fig. 3d) and measured the distance between OPC somata and bright, c-Fos-expressing neurons. In CA1, this distance was significantly shorter in dcz-injected mice compared with the vehicle controls (Fig 3e). The same trend was observed in CA2/3, but the difference was not significant (Fig. 3f). Next, we used the Imaris ‘spots’ tool to seed spots on OPC processes and then measure the number of spots within a radius of 4µm from the surface of the c-Fos+ neuron vehicle (Fig. 3g) and dcz (Fig. 3h) treated animals (scheme in Fig. 3i). Again, there was a significantly higher number of spots detected close to the neurons in CA1 (Fig. 3j), and there was the same trend observed in CA3 but without significance. There was no difference in the number of OPC processes in CA1 or CA3 of mice injected with vehicle or dcz (Extended Data Fig. 4).

These observations suggest that OPCs approach active neurons in the hippocampus of adult mice and move their processes towards them. The phenomenon of OPC processes encircling active neurons appears to occur in response to a variety of conditions that lead to hyperexcitability of principal neurons at different ages, and the degree to which OPC processes altered their morphology and extended their processes toward and surrounded active neurons seemed to be correlated with the magnitude of neuronal activation.

OPCs influence the activity of neurons in close proximity to their processes

In order to address the physiological significance of the OPC-neuronal soma interactions we observed, we prepared acute slices from neonate NG2DsRed mice (at P4) to visualize OPCs (Fig. 4a). Neuronal activity was monitored by 2-photon microscopy after bath incubation of the slices with the calcium-indicator Cal520 (Fig. 4b). Calcium transients were recorded in the hippocampal pyramidal layer, and the changes in fluorescence intensity (ΔF/F) were measured (Fig. 4c). From the recorded neurons, the value of the average change in fluorescence was compared between neurons directly in contact with OPCs (Fig. 4d) and neurons without any OPC contact (Fig. 4d). Neurons with OPC contact had significantly lower average values for ΔF/F compared with those without apparent OPC contact (Fig. 4e), indicating that OPCs may be able to influence neuronal activity by surrounding the soma with their processes.

Transcriptomic changes in Scn1a mutant hippocampus

To explore the nature of molecular signaling between active neurons and OPCs that led to OPC process extension around the somata of active neurons, we analyzed publicly available bulk RNA-seq data generated from the hippocampus of P15 Scn1a control and mutant mice (GSE149754) (Fig. 5a), with 3 biological replicates. Initial DESeq2 analysis yielded only 4 genes that were differentially expressed at p-adj < 0.05. Principal component analysis of all 6 samples revealed clustering of Scn1a control 1 (cont1) and cont2, but cont3 had limited clustering with the other two control samples. Similarly, Scn1a mutant 1 (mut1) and mut3 clustered together, but mut2 did not cluster with either of the other mutant samples (Fig 5b).

All samples were then compared to another genetic epilepsy mouse model F1.*Scn1a*$^{+/-}$ which observed mutant mice with and without seizures, to determine if mut2 was potentially demonstrating and extreme phenotype regarding seizures, as opposed to other physiological events (Hawkins et al., 2018). Principal component analysis with the P24 samples with limma batch effects adjustment made clear that mut2 continued to act as an outlier and did not segregate with any samples including the seizing mutants (Figure 5c)(DESEQ2, limma). Based on these results we determined that mut2 should be regarded as a sample that experienced an increased physiological response and was excluded as an outlier from the subsequent analysis, whereas cont3 was kept in. When DESeq2 analysis was performed on the remaining samples after excluding mut2, we found 184 differently expressed genes with *p-adj* < 0.05, of which 150 were upregulated (Fig. 5d, Extended Data Table 2). The majority of

the genes that were upregulated with *padj* < 10^-5 and log2FoldChange > 1 were genes encoding extracellular matrix proteins and integral membrane proteins, including growth factor binding proteins, transporters, and membrane receptors. Among the prominently upregulated genes was *Mgp* (encoding matrix G1a protein), while *Gpr22* (encoding an orphan G-protein coupled receptor) and *Trhr* (encoding thyrotropin releasing hormone receptor) were among the downregulated (Fig. 5d). *AVP* encoding arginine vasopressin had the highest log2FoldChange value of 7.2 caused by high expression in the mutant samples and nearly no expression in the controls, resulting in p-adj of 1.94E-05.

Analysis of GO (gene ontology) terms enriched among upregulated genes in the mutant hippocampus revealed a high representation of extracellular matrix (ECM) proteins, particularly collagens, including *Col6a1* and *Col6a2* encoding alpha1(VI) and alpha2(VI) subunits of type VI collagen (Col6a1, Col6a2), respectively. ECM-receptor interaction was the most highly represented KEGG (Kyoto Encyclopedia of Genes and Genomes) pathway, along with TGFβ signaling pathway, *a*nd extracellular matrix structural constituent along with collagen binding were the most prominently enriched GO Molecular Function (MF) term. The GO Cellular Component (CC) terms extracellular matrix and collagen-containing extracellular matrix were also highly represented. Type VI collagen is a well characterized binding partner for NG2 (Stallcup et al., 1990; Tillet et al., 1997) and could be involved in attracting NG2-expressing OPC processes to active neurons.

Expression of Collagen VI in mutants

To verify the increased expression of collagen VI in hyperexcitable neurons, we isolated neurons from the hippocampus of E18 mice carrying the Scn1a mutation and controls. After 8 days in culture, neurons were stained for the expression of collagen VI protein by immunocytochemistry (Extended Data Fig. 5a). The fluorescence intensity on neuronal somata was assessed (circles in Extended Data Fig. 5 b,c) and compared between neurons isolated from mutant and control mice. Mutant neurons showed a significantly higher expression of collagen VI (Extended Data Fig. 5d), verifying our results obtained from the RNA analysis.

Next, we examined C6a1/2 expression on 15-µm thin cryostat sections of P15 Scn1a control hippocampus. C6a1 or C6a2 revealed more punctate pattern of collagen VI, which was often co-localized with PDGFRα+ OPC processes (Extended Data Fig. 6c-d). C6a1 was also detected on blood vessels (Extended Data Fig. 6c), as predicted from previous studies (You et al., 2014). Comparison of C6a1 immunofluorescence in Scn1a control and mutant hippocampus revealed stronger signal in the mutant, and the

C6a1+ puncta were often colocalized with PDGFRα+ OPC processes (Extended Data Fig.6e).

We further aimed to investigate the effect of TGFß, which was elevated in our screens, and two members of the TGFß-superfamily on OPCs: BMP7 (bone morphogenetic protein 7), which has previously been shown to inhibit OPC differentiation (Petersen et al., 2017) and to promote migration of OPCs (Choe et al., 2004), and ActivinA, which has been reported to promote OPC differentiation (Miron et al., 2013).

OPCs were isolated from wild type mouse neonates and cultured with the addition of the cytokines. We then assessed the surface covered by OPCs in each condition with the Imaris surface feature (Extended Data Figure 7). This parameter is an indicator for the extend of number and complexity of processes and growth cone-like structure formation OPCs form in culture dishes. The average area covered by OPCs was increased in response to BMP7, but not TGFß or ActivinA, when comparing all 3 cytokines to the control (Extended Data Fig. 7a). Specifically, the addition of ActivinA did not result in an increase in the area covered by OPCs (Extended Data Fig. 7b and f) when compared to the control (example shown in Extended Data Fig. 7e). The addition of BMP to the culture medium resulted in a significant 1,6-fold increase of the average area taken by OPCs (698.2µm² vs. 1101µm², Extended Data Fig. 7c and g). In standard OPC proliferation medium, TGFß did not increase the surface area of OPCs. However, when NT3 was omitted from the culture medium, TGFß significantly increased the area covered by OPCs in culture (Extended Data Fig. 7d and h). NT3 has been shown to promote OPC process outgrowth and differentiation of OPCs before (Siebert and Osterhout, 2021) and thus seems to mask the effects of TGFß.

DISCUSSION

Morphological changes in OPCs in response to increased neuronal activity

OPCs respond to neuronal activity and have been shown to be able to detect release of neurotransmitters and ATP along axons, which induce proliferation or differentiation into OLs (Bergles et al., 2000; Gibson et al., 2014; Kukley et al., 2007; Nagy et al., 2017; Wake et al., 2015; Ziskin et al., 2007). We observed that OPC processes are frequently localized around the soma of neurons in the pyramidal layer of the hippocampus, as well as next to and around the AIS. To address the functional impact of this relationship, we examined the changes in the spatial relationship of OPCs and hippocampal neurons in response to altered neuronal excitability. We used a mouse model of Dravet's syndrome, which was initially described as severe

myoclonic epilepsy of infancy and is now known as a channelopathy with most of the affected patients carrying mutations in the *SCN1A* gene (Dravet et al., 2011). The *SCN1A* gene encodes the voltage-dependent Na^+ channel $Na_v1.1$ and is expressed mainly in inhibitory neurons. Loss of function mutations in the *SCN1A* gene lead to impaired inhibition and an overall increase in the excitability of the network.

We found that OPC processes were more prominently extended around c-Fos+ neurons, not only in the mutant but also in control hippocampus, compared to c-Fos-negative neurons in CA1. Upregulation of the immediate early gene c-Fos is considered to be a marker of neuronal activity (Morgan & Curran, 1991). Furthermore, we observed OPC processes wrapping around chemogenetically activated neurons in the adult hippocampus, implying that this is not a developmental or pathological phenomenon. Our observations indicate that OPCs detect and dynamically respond to focal changes in neuronal activity.

The increased complexity of OPCs around activated neurons was not accompanied by increased OPC density or proliferation, contrary to previously published studies. For example, OPCs proliferate after electroconvulsive seizures induced in the rat (Wennstrom et al., 2003). Optogenetic stimulation of the cortex led to a 4-fold increase in OPC proliferation within 3 hours (Gibson et al., 2014; Li et al., 2010), and selective optogenetic stimulation of OPCs led to increased OPC density and proliferation (Oishi et al., 2023). Direct daily electrical stimulation of the pyramis for 10 days led to increased BrdU incorporation into OPCs in the contralateral corticospinal tract of the spinal cord (Li et al., 2010). The difference could be due to differences in the magnitude and duration of the hyperexcitable state of the pyramidal neurons. Scn1 mutant mice did not show abnormal behavior until P14, consistent with the previous report (Kuo et al., 2019). In Scn1a+/- heterozygous mutants, parvalbumin-expressing interneurons show normal firing through postnatal day 10 (P10) followed by a sudden onset of reduced firing rate at P11 (Favero et al., 2018). Thus, the relatively short duration of the mildly hyperexcitable state may not have been sufficient to elicit a proliferative response. The short lifespan of the Scn1a mutant mice precluded analysis beyond P15.

OPC processes undergo changes in a variety of physiological and pathological conditions (Ong & Levine, 1999) and display regional and age-dependent differences in their size, morphology and passive membrane properties (Chittajallu et al., 2004; Spitzer et al., 2019). In vivo, OPC processes are dynamic and sensitive to changes in their surrounding environment (Chapman et al., 2023; Hughes et al., 2013; Hughes et

al., 2018). A recent report showed a reduction in the number and branching of OPC processes when excitatory synaptic transmission was blocked by botulinum toxin A (BoNT/A), which cleaves the synaptic membrane protein SNAP-25 (Binz et al., 2010; Chacon-De-La-Rocha et al., 2021). Another recent study showed a selective increase in the complexity of OPC processes in the cortex of patients with schizophrenia as well as in a mouse model of schizophrenia (McCutcheon et al., 2020; Yu et al., 2022). It has been suggested that excitation/inhibition imbalance due to reduced inhibitory input to pyramidal neurons in the prefrontal cortex contributes to the pathophysiology of schizophrenia (McCutcheon et al., 2020).

The ability of OPCs to dynamically redirect their process toward active neurons suggests that they have a mechanism to detect changes in the activity of nearby neurons and transduce the information into a molecular signal that results in cellular changes. OPCs express receptors for glutamate and GABA and respond to neurotransmitters at synaptic and extrasynaptic sites. Although the consequences of OPC activation by neurotransmitters remain unclear, it is presumed that Ca^{2+} signal is involved, as Ca^{2+}-permeable AMPA receptors are activated in neuron-OPC synapses (Ge et al., 2006), and changes in Ca^{2+} levels were shown to influence proliferation and differentiation of OPCs (Chen et al., 2018). The voltage-dependent Ca^{2+} channel $Cav_{1.2}$ is activated by OPC membrane depolarization (Cheli et al., 2016). Moreover, *Nfat4*, which is activated by the calcium-dependent protein phosphatase calcineurin, affects their differentiation by promoting myelin gene transcription (Weider et al., 2018). However, the specific signaling pathways that are involved in neuron-OPC interplay under hyperexcitable conditions have remained unknown.

Our Analysis of GO (gene ontology) terms revealed a high representation of collagen VI, which we could observe in neurons cultured from Scn1a mutant mice. While it is possible that OPCs bind to the increasingly available extracellular matrix protein collagen VI upon neuronal activity via NG2, the exact mechanisms behind the close proximity and the molecules stabilizing these interaction remain to be determined. Soluble proteins released by over-active neurons may also cause changes in morphology of OPCs. We found an effect of BMP-7 on the surface expansion of OPCs in culture, indicating process expansion. It will be interesting to investigate changes in other molecular cues that determine OPC mobility.

OPCs cause a reduction in activity in neurons whose soma they contact

What consequence has the surrounding by OPC processes for the affected neurons? We detected a significant reduction in Ca^{2+} transients in neurons that were in

close proximity to OPCs, surrounded by their processes. These findings indicate that OPC processes, initially directed towards active (c-Fos+) neurons, dampen neuronal activity by surrounding the targeted neuron. Although the exact mechanism how OPCs achieve to reduce neuronal activity is unsolved, it could be mediated either by physical contact reducing the signals or solutes that reach the neuron, or it could be mediated by active release of signaling molecules by OPCs that in turn cause intracellular changes in the contacted neuron. The observation that OPCs frequently and across developmental stages approach the soma of neurons is new, and aligns with other recently published studies implying that OPCs exert additional functions independent of myelination (Auguste et al., 2022; Fang et al., 2025; Kirby et al., 2019; Xiao et al., 2022). We recently observed interactions between OPCs and the soma of dopaminergic neurons in the *substantia nigra pars compacta* in mice of different age groups (Fitzgerald et al., 2025), indicating that it is a widely occurring interaction. Quite recently, another study described the formation of contact between OPCs and neuronal soma in an activity dependent manner. In this study, the authors found that these contacts facilitated exocytosis of neuronal lysosomes, having an impact on neuronal metabolism (Fang et al., 2025). Interestingly, microglia have recently been shown to form specialized somatic purinergic contacts with neurons (Cserep et al., 2020). These contacts can modulate neuronal activity by suppressing neuronal activity (Badimon et al., 2020) and exert a neuroprotective role during homeostasis and more pronounced after brain injury (Cserep et al., 2020). Our results that neurons in close proximity to OPCs had lower Ca^{2+} fluxes as compared to those without OPC contact indicate that OPCs exert regulatory functions with regard to neuronal activity in addition to microglia, the mechanism of which needs further research.

In line with our results on elevated expression of collagen VI in Scn1a mutant mice and a potential neuroprotective role for OPCs, collagen VI was found to be increased in the hippocampus in a mouse model of Alzheimer's Disease, which had a neuroprotective effect (Cheng et al., 2009). More recently, collagen VI was detected to be upregulated after the occurrence of seizures in cortex and hippocampus in a mouse model of epilepsy and in brain tissue from human patients suffering from epilepsy, which reduced the overall network excitability (Ramos-Moreno et al., 2024). The binding of NG2 on OPCs could be a link between overexpression of collagen VI and OPC mediated decrease in neuronal activity.

In summary, our detailed cellular analysis revealed local reorientation OPC processes to navigate toward active neurons with increased perineuronal collagen VI. Sequencing analyses demonstrated increased ECM and altered TGFβ signaling in the

hyperexcitable brain, accompanied by OPC-specific changes suggesting their response to the altered ECM and TGFβ. Moreover, we show that the close proximity of OPC processes to the soma of active neurons in turn reduces their changes in intracellular calcium elevations, suggesting a protective mechanism of hyperexcitable neurons. These findings indicate that OPCs are an active and integral part of the neural network that responds dynamically to altered neuronal excitability. Future studies may be directed toward elucidating the specific molecular signals mediated through interplay between different cell types and how they coordinate neuronal excitability.

MATERIALS AND METHODS

Animals

Homozygous Vgat-ires-cre knock-in mice (Jax #028862; *Slc32a1*$^{tm2(cre)Low/}$ (*Vgat*$^{cre/cre}$) (Vong et al., 2011) were crossed with heterozygous Scn1a-A1783Vfl/+ mice (Jax #026133; *Scn1a*$^{tm1.1Dsf/J}$ (*Scn1a*$^{A1783/+}$) carrying a dominant, cre-dependent loss-of-function mutation Scn1a^{A1783V} allele (Kuo et al., 2019; Ricobaraza et al., 2019). We used both sexes of *Vgat*$^{cre/+}$*;Scn1a*^{A1783V}/$^{+}$ mice and the littermates *Vgat*$^{cre/+}$*;Scn1a*$^{+/+}$ as control. In some cases, 50 µg/g EdU (5-ethynyl-2'-deoxyuridine, Cayman Chemicals #20518) was injected intraperitoneally 2 hours before perfusion. For chemical activation of adult mice, Camk2a-cre (T29-1) tg/+; CAG-LSL-Gq-DREADD (CAG-CHRM3-mCitrine) tg/+ double transgenic mice were injected with 100 µg /kg deschloroclozapine (dcz) or vehicle and the brains harvested 6 hours later

All animal procedures were approved by the Institutional Animal Care and Use Committee of the University of Connecticut. Both sexes were used for all experiments.

Hippocampal neurons were isolated from from B6(Cg)-Scn1atm1.1Dsf/J X 129S1/Sv-Hprttm1(CAG-cre)Mnn/J mouse brain. OPCs were isolated from C57BL/6 wild type mice. These experiments were performed in accordance with the German Animal Welfare Law and the allowance of the (local) authorities(Regierungspräsidium Tübingen).

Tissue processing

For immunofluorescence labeling, P14/P15 or adult mice were perfused and fixed with 4% PFA containing 0.1M L-lysine and 0.01M sodium meta-periodate (PLP) (Pfeiffer et al., 2021). After perfusion, animals were dissected and brains post-fixed in PLP fixative for 1-2 hours and then washed 4 times in 0.2M sodium phosphate buffer, pH7.4. The brains were incubated in 30% sucrose in 0.2M sodium phosphate buffer for at least 48 hours and then frozen in OCT compound (Tissue-Tek; Adwin Scientific 14-373-65). 15-µm sections were cut on a Leica CM3050S cryostat. For the detection of extracellular matrix (ECM) after chemogenetic stimulation of hippocampal neurons, we perfused the mice, postfixed and rinsed the brain as above, and cut 50-µm sections on a Leica VT1000S vibrating-blade microtome.

Immunohistochemistry

For immunolabeling, sections were rinsed in PBS, blocked in 1% bovine serum albumin (BSA) containing 0.3% Triton X-100 in PBS for 1 hour at room temperature, followed by overnight incubation with primary antibodies diluted in 1% BSA/0.1% Triton

X-100 in PBS. The sections were rinsed 3 times in PBS and incubated in the secondary antibodies diluted in 1%BSA/0.1%Triton X-100 in PBS at room temperature for 1 hour. The source and dilution of primary and secondary antibodies are listed in Extended Data Table 1. Sections were rinsed and mounted with Vectashield containing DAPI (Vector, H-1200) or ProlongGold (InVitrogen).

To detect EdU, immunolabeled sections were washed 3 times with PBS and incubated in the Click reaction mixture containing 150mM NaCl, 100mM TrisHCl pH 7.15, 4 mM $CuSO_4.5H_2O$ (Sigma, C6283), 4 ng/mL Alexa Fluor-647-conjugated azide (ThermoFisher, A10277), and 100mM sodium ascorbate (Sigma, A4034) at room temperature for 30 min. The sections were then washed three times in PBS, stained with 5 µg/mL Hoechst 33342 in PBS (InVitrogen Molecular Probes, LSH3570), and mounted in Vectashield without DAPI (Vector, H-1000).

2.5. Fluorescence microscopy and image analysis

Images of fluorescently labeled tissue sections were acquired using a Zeiss Axiovert 200M microscope with Apotome or a Leica SP8 confocal microscope from CA1 region in the hippocampus. For images obtained with the 40x objective, *z*-stacks were taken at 0.35µm *z*-step size using Zeiss Axiovert or Leica LAS X software. Images were analyzed with the Leica LAS X (for 3D reconstruction) ImageJ2 (Fiji, version 1.53a) and Imaris v10.0 (Oxford Instruments, UK).

For fluorescence intensity measurements, all images acquired on the Leica SP8 confocal microscope with the same laser intensity, gain, and resolution and a step size of 0.35 µm using a 40x objective. ImageJ2 fluorescence intensity of PDGFRα-signal was processed as follows: the values from a constant number of z-stacks in an area of 52,007.876 square pixels, was combined (sum slices), background was subtracted (rolling ball radius of 50 pixels), and the ‘mean gray value’ for the entire field in each image was measured. The value for the control image from the same sample, where the primary antibody had been omitted, was subtracted. GraphPad Prism 9 was used to perform statistical analyses.

3D rending, surface reconstruction, automated Sholl analysis and spot seeding was performed with Imaris v10.2 (Oxford Instruments, UK). GraphPad Prism 10 was used to perform statistical analyses.

The STED image in Figure 1k was acquired using a Leica SP8 Gated STED 3X confocal microscopy system (Yale University School of Medicine Center for Cellular and Molecular Imaging).

Sholl analysis

Images were acquired using a Leica SP8 confocal microscope (Leica Microsystems, Germany) with a 40x objectives with a resolution of 1024x1024 pixels. 55 z-stacks were taken at a z-step size of 0.35µm. 3D reconstructions were generated with Imaris 10.0 (Oxford Instruments, UK). After converting the lif-files, filaments were reconstructed using the filaments function. To better visualize the filaments that have been traced back to a specific OPC, color coding using 'Filament ID' was used.

Sholl analysis was performed on the filaments reconstructed with Sholl spheres set to 1µm. Intersections up to 40µm away from the cell center were taken into account.

Measuring the distance between neurons and OPCs

For the analysis of the distance between active neurons and OPC soma, a distance channel was created as the Intensity Center Channel 3 via the distance transformation function that is supported by MATLAB, found in the surfaces section.

To analyze the number of branches interacting with the active neurons, the Imaris spots module was used. Spots were placed on filaments with auto-depth. The diameter of the spots was set as 0.4, and machine learning was trained to eliminate the spots planted on the soma of OPCs. To reconstruct the active neurons, the surface function was used. To distinguish cFOS positive neurons from cFOS negative neurons, the feature was trained with machine learning. The average distance to 3 nearest neighbors filter was set to 8.01µm. Thereafter, the Intensity Center Channel 3, which is the distance channel, was added as a filter and the maximum distance for the spots to be included was set to 4 µm. The number of the spots that are found in the distance of 4 µm maximum limit was extracted to be compared for the clozapine-treated and vehicle-treated images. The statistical analysis was performed on GraphPad Prism 10.2.3.

Calcium-imaging in acute slices

Hippocampal slices were prepared from P4 NG2DsRed transgenic mice. Mice were decapitated and the brain hemispheres rapidly dissected and placed in ice-cold bicarbonate-buffered extracellular solution (125mM NaCl, 4.5 mM KCl, 2mM $CaCl_2$, 1mM $MgCl_2$, 1.25mM NaH_2PO_4, 26mM $NaHCO_3$, 20mM glucose, pH 7.4 when bubbled continously with 95% O_2 and 5% CO_2). 500µm thick transverse hippocampal slices were cut with a vibratome ad kept at 34°C at least for one hour before recording in a storage chamber containing extracellular solution and bubbled with 95% O_2 and 5% CO_2.

Fluorometric Ca^{2+} measurements were performed in slices after bath incubation with membrane permeant acetoxymethyl ester of Cal-520™ (Cal-520™ AM, AAT Bioquest) in oxygenated extracellular solution for 10 minutes at 37°C. Cal-520™ AM-loaded slices

were placed in a recording chamber and imaged with an upright laser scanning microscope (FV300; Olympus, Japan) coupled to a mode-locked Ti:sapphire laser (710-990nm excitation wavelength, Mai Tai; Spectra Physics, USA) equipped with a 40x water-immersion objective (NA 0.8, Nikon, Japan). Cal-520™ AM and DsRed were excited at 925nm and emitted light split at 585nm. During the recording, the slices were continously perfused with standard extracellular solution at 32-34°C.

Recordings were obtained from the pyramidal layer of the hippocampus (Garaschuk et al., 1997; 1998). OPCs were identified based on their red fluorescence and morphology. Fluorescent signals were obtained from the cell bodies of different pyramidal cells and the background fluorescence was measured in parallel in a separate region near the cells of interest and used for correction of the fluorescent signal. ROIs were defined with ImageJ2 (Fiji) and traces analyzed with Igor Pro 8 (Wave metrics).

2.7. Analysis of published RNA-seq dataset of Scn1a control and mutant hippocampus

We used the RNA-seq dataset GSE149754 from P15 *Vgat*$^{cre/cre}$*;Scn1a*$^{+/+}$ (control) and *Vgat*$^{cre/cre}$*;Scn1a*$^{A1783V/+}$ (mutant) mice. The samples consisted of 3 biological replicates comprised of 2 females and 1 male for each genotype. Sequence files were downloaded to a local server, Illumina adapters were trimmed using TrimGalore! (v.0.6.5, doi: 10.5281/zenodo.5127898), and low quality reads were filtered out. The filtered reads were aligned to the Ensembl mm10 reference genome with annotations (release 102) and gene counts quantified using the STAR (Spliced Transcripts Alignment to a Reference) software (v.2.7.1a) (Dobin et al., 2013). Transcripts were assembled and estimated abundances quantified using HTseq (v0.11.3). The counts were then analyzed for differential gene expression in R (v.4.0.3) using the DESeq2 package (v.1.30.0) (Love et al., 2014). GO analysis was performed using the enrichGO function of clusterProfiler (v3.6), (Yu et al., 2012) in R, as well as with the web version of g:Profiler (Raudvere et al., 2019; Reimand et al., 2016) and the GSEA (Gene Set Enrichment Analysis) software using the mouse gene set collections (mouse MSigDB v2023.1) (Liberzon et al., 2015; Subramanian et al., 2005).

2.8. Bulk ATAC-seq and RNA-seq of OPCs from Scn1a control and mutant cerebral cortex

OPCs were immunopurified from the cortex of P14-15 *Vgat*$^{cre/cre}$*;Scn1a*$^{+/+}$ (control) and *Vgat*$^{cre/cre}$*;Scn1a*$^{A1783V/+}$ (mutant) mice as previously described (Sherafat et al., 2021). Briefly, cortices were incubated in papain solution (Worthington) at 35°C for 5 min, taken out to remove meninges, and then incubated an additional 10 min in papain solution. Tissue was triturated and OPCs captured using a PDGFRα antibody-coated

dish. Cells were trypsinized, spun, and resuspended in panning buffer. Dead cells were removed by FACS after DAPI labeling. Cells were used immediately for ATAC-seq library preparation or frozen as cell pellets for RNA extraction. Three biological replicates were used for each condition for all three sets of sequencing. OPCs from both males and females were mixed in each biological replicate.

For ATAC-seq, 50,000 cells were used per reaction. Libraries were created following the Omni- ATAC protocol (Corces et al., 2017) using Nextera Tn5 transposase enzyme. Libraries were amplified using previously provided primers (Buenrostro et al., 2015). Sequencing of ATAC libraries were performed by the Center for Genome Innovation (University of Connecticut). Samples were run on the Illumina NextSeq (version 2.5, Mid output 150 cycle) for paired end reads averaging 75. Adaptors were trimmed using TrimGalore! (v0.6.4), and filtered reads were mapped to the mouse mm10 reference genome using Bowtie2 (v2.4.1), and peak-calling was performed using Genrich. Mitochondrial sequences and reads aligning to Chromosome Y were removed through Genrich (v0.6) prior to calling peaks. Raw counts for peaks were generated using featureCounts in R (v3.2.2). Peaks located at gene promoters were defined as +/- 500 bps from transcription start site. Genome-wide annotations were found using ChIPSeeker (v3.10) (Yu et al., 2015) Bioinformatics QY. For genomic feature characterization, promoters were defined as +/- 3 kb from TSS. Transcription terminal site (TTS) was defined as 3 kb from the end of the last exon of a gene. Differential expression analysis was performed with NOISeq in R (Tarazona et al., 2015) NAR. GO enrichment analysis was performed using the web version of g:Profiler (Raudvere et al., 2019; Reimand et al., 2016).

For RNA- seq, frozen OPC pellets were homogenized with a syringe needle and lysed with buffer provided by the RNA PureLink Mini kit (Promega), and RNA was extracted following manufacturer's protocol. All RNA samples had RIN values of 7.3 or higher. RNA library generation and sequencing were performed by the CGI using Illumina Stranded Total RNA Library Preparation Kit. They were sent to Macrogen for sequencing on the HiSeq for 150-bp paired end reads. Illumina adapters were trimmed from 3' end of raw reads using TrimGalore! (v0.6.4). Reads were aligned to the mouse mm10 reference genome using Bowtie2 (v2.4.1). Transcripts were assembled and estimated abundances quantified using HTseq (v0.11.3). Differential expression analysis was conducted with DESeq2.

To visualize gene networks with altered expression and chromatin accessibility we used Cytoscape_v3.10.0 (Shannon et al., 2003) to integrate the GO terms that were

enriched in Scn1a mutant hippocampal tissue RNA-seq, OPC ATAC-seq, and OPC RNA-seq.

Primary cell culture neurons

Hippocampal neurons were isolated from embryonic day 17 (E17) from B6(Cg)-Scn1atm1.1Dsf/J X 129S1/Sv-Hprttm1(CAG-cre)Mnn/J mouse brain. After killing the pregnant female with CO_2, embryos were removed and decapitated. The hippocampus was removed microsurgically, and the tissue pieces were washed three times in 4°C magnesium- and calcium-free HBSS (PAA Laboratories GmbH) before they were treated with 2.5% trypsin for 15 minutes at 37°C. Thereafter, tissue pieces were rinsed with DMEM containing 10%fetal bovine serum (Biochrom, AG), L-glutamine (Invitrogen) and penicillin/streptomycin (Invitrogen) to block the trypsin reaction. Neurons were dissociated mechanically by using a pipette and a cell strainer (Becton Dickinson). 150.000 cells were plated per poly-D-lysine-coated 4-well labtek and maintained in Neurobasal medium (Gibco) supplemented with B27, glutamine and penicillin/streptomycin (all Invitrogen).

After 8 days in culture, cells were fixed by adding 0.5% PFA in PBS for 10 minutes. After washing 3 times with PBS, cells were incubated with primary antibodies to collagen 6 (#180855 and #182744, both from Abcam), diluted 1:500 in 1% BSA and 0.1% Triton-X in PBS overnight at 4°C. The next day, cells were rinsed 3 times in PBS and incubated with the sedondary antibody (donkey anti-rabbit Alexa 647, Jackson Immuno Research), diluted 1:1000. After washing for another 3 times with PBS, cells were incubated with DAPI (diluted 1:4000 in PBS) for 8 minutes, washed again and stored in PBS at 4°C until imaged with an inverted Zeiss LSM 700 confocal microscope equipped with a 40X/1.3 NA oil immersion objective. ROIs were defined and fluorescence intensity measured with ImageJ2 (Fiji).

ACKNOWLEDGEMENTS

We thank Youfen Sun for maintaining the animal colony and Owen Greene for his assistance with cytokine immunofluorescence analysis on tissue sections. We thank Dr. Chris O'Connell, Director of Advanced Light Microscopy Facility, for his assistance with the Leica SP8 confocal microscope, which was purchased with funds from an NIH Instrumentation Grant S10 OD016435 (PI: Akiko Nishiyama). We thank Dr. Bo Reese in the Center for Genome Innovation for her help with RNA and ATAC-sequencing and Dr. Vijender Singh for his help with bioinformatic analysis of sequencing results. We

thank Dr. Olga Oleksiuk at the HIH CIN Imaging Cluster, Tübingen, for support with using the microscopes (Leica SP8 and Zeiss 710).

The work was supported by the European Union's Framework Program for Research and Innovation Horizon 2020(2014-2020) under the Marie Sklodowska-Curie Grant Agreement No. 845336 to FP and grants from the National Institutes of Health NIH R01NS073425 and R01NS116182 to AN.

Figures

Figure 1

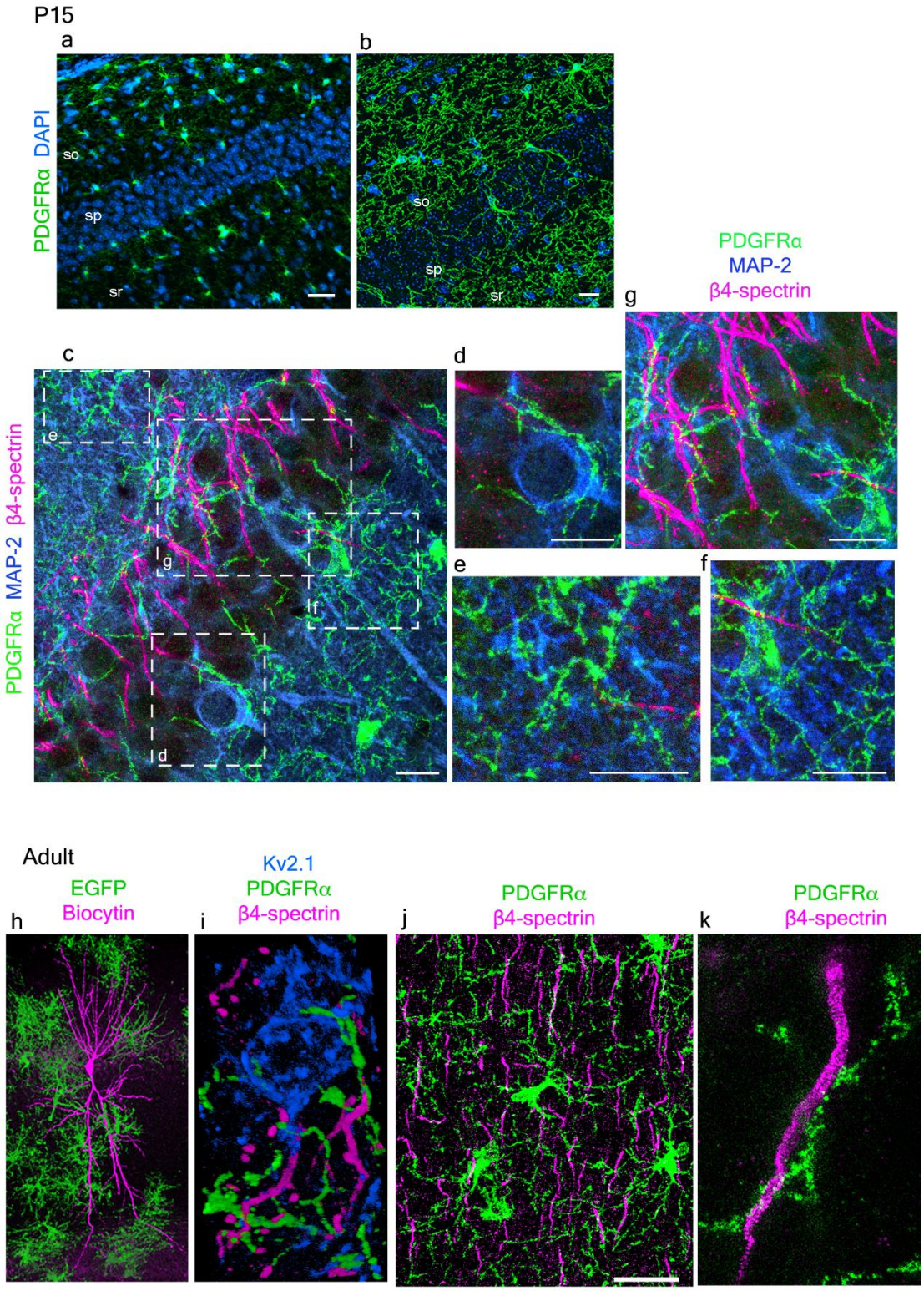

Figure 1. OPC processes in close proximity to pyramidal neuronal subdomains in P15 hippocampus.

a. Immunofluorescent image of the CA1 hippocampal region showing the distribution of OPCs (stained with anti-PDGFRα antibody in green) in stratum oriens (so), stratum pyramidale (sp), and stratum radiatum (sr). DAPI is shown in blue for better orientation. Scale bar represents 50µm.

b. confocal images showing OPCs (stained with anti-PDGFRα antibody in green) inserting processes into the sp. Scale bar represents 20µm.

c-g. Immunolabeling for PDGFRα showing the distribution of OPCs in stratum oriens (so), stratum pyramidale (sp) and stratum radiatum (sr) of hippocampal CA1 region and the localization of their protrusions. Neuronal parts are stained with ßIV spectrin (magenta), MAP-2 (blue). Scale bar represents 15 µm. d-g show zoomed in areas indicated by white boxes in c.

h. Biocytin (magenta) filling of a pyramidal neuron in a PDGFRα GFP (green) transgenic mouse shows numerous OPC processes intermingled with neuronal processes and cell body. Scale bar represents

i. OPC processes (stained with anti-PDGFRα antibody in green) around the soma of a neuron expressing Kv2.1 (shown in blue) and the AIS (stained with anti-ß4-spectrin in magenta). Scale bar represents

j. OPCs (stained with anti-PDGFRα antibody in green) interacting with neurons and their AIS (stained with anti-ß4-spectrin in magenta). Scale bar represents

k. high magnification (STED microscopy) showing OPC processes (stained with anti-PDGFRα antibody in green) twisted around the AIS (stained with anti-ß4-spectrin in magenta).

Figure 2. OPC processes preferentially contact c-Fos+ active hippocampal CA1 neurons.

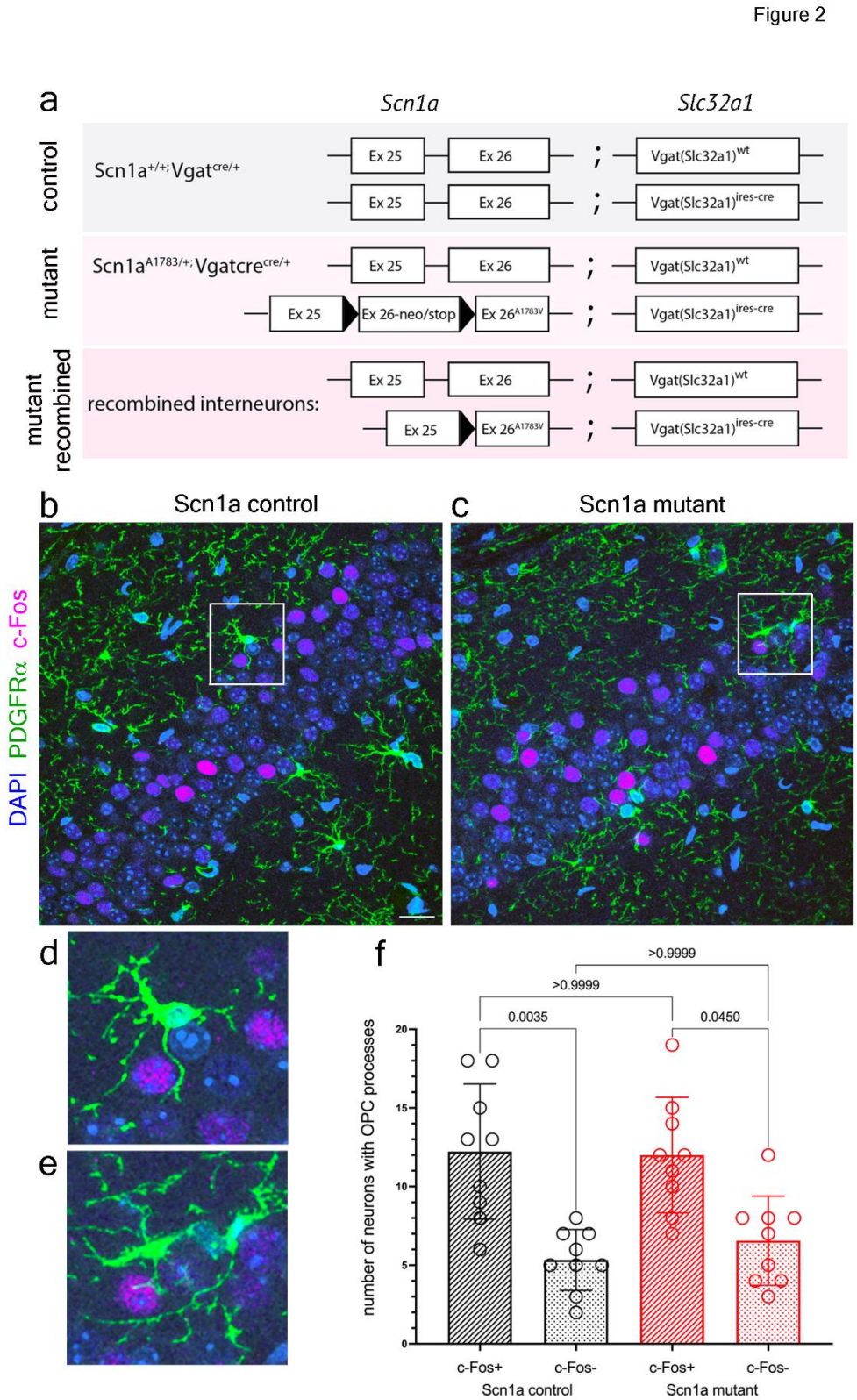

a. A schematic showing *Scn1a* and *Slc32a1 (Vgat)* alleles in Scn1a control (gray) and Scn1a mutant (pink) mice. Ex 25 and Ex 26 represent exons of the *Scn1a* gene. Genotype in the middle (light pink) shows before recombination. Bottom in darker pink shows genotype in recombined interneurons expressing Cre. Black triangles, loxP sites.

b-e. Confocal images of CA1 in Scn1a control (b) and mutant (c) mice showing OPC processes (green, PDGFRα+) and c-Fos+ (magenta) active neurons in stratum pyramidale. Nuclei are labeled with DAPI (blue). Boxed areas in b and c are enlarged in d and e, respectively to show OPC processes around c-Fos+ neurons. Scale bar 20 µm. Images represent maximum projections of 11 *z*-stacks spanning 3.85 μm.

f. Number of neurons in CA1 with 5-10 OPC processes detected within 10µm from the soma center (detected by Sholl analysis). 5 images per mouse (n=3) were analyzed. Kruskal-Wallis test with Dunn's multiple comparison test was performed.

Figure 3. OPCs approach active neurons upon activation in the adult hippocampus.

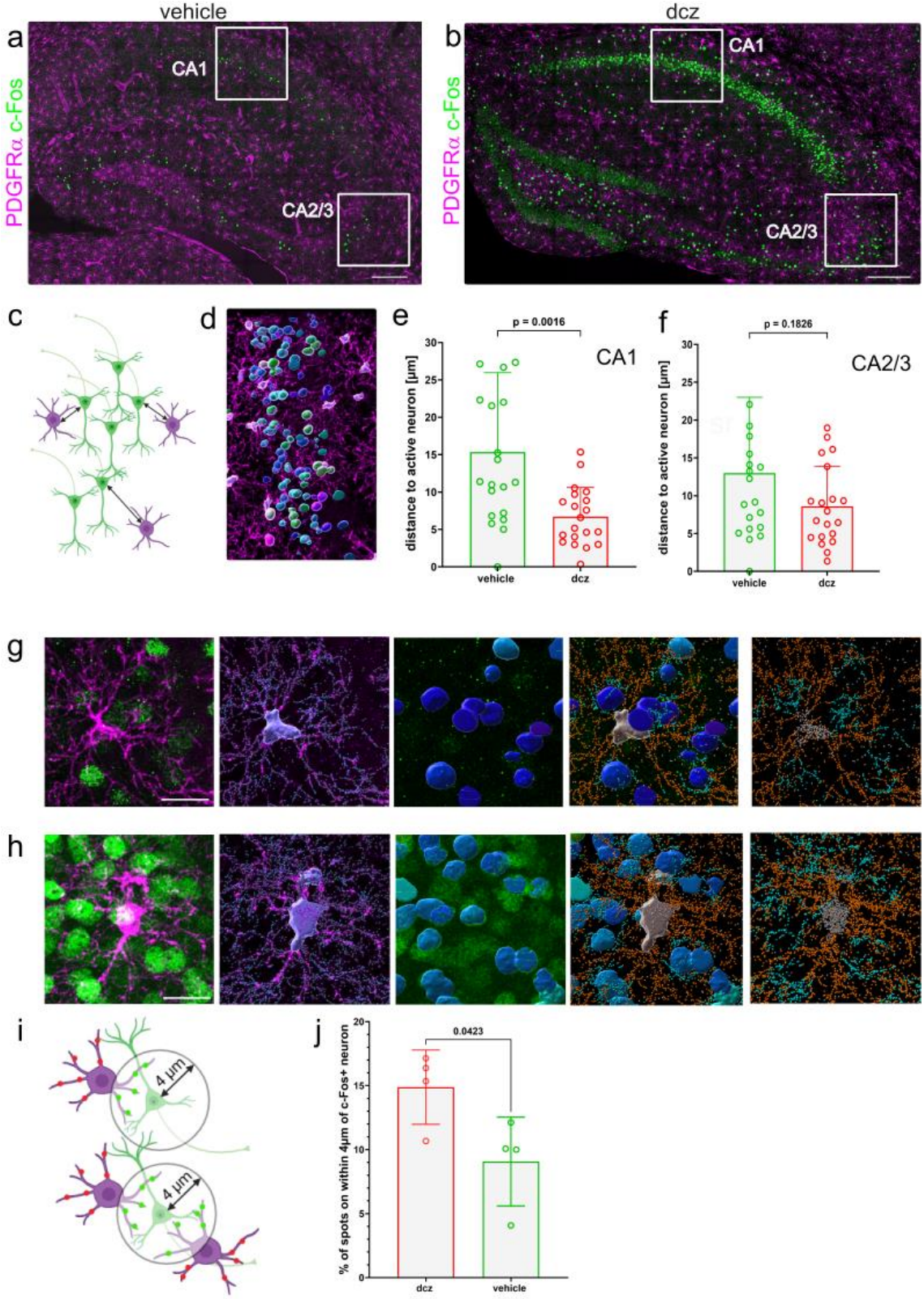

a-b. C-Fos (green) expression 6 hours after vehicle (a) or dcz (b) injection in the hippocampus of adult mice. OPCs are labeled with anti-PDGFR□ antibody (in magenta). White boxes show CA1 and CA2/3 regions, respectively, that were further analyzed. Scale bars represent 200µm.

c. Scheme showing how the distance between the soma of OPCs and the nearest c-Fos+ neuronal soma was measured.

d. Imaris reconstruction of the c-Fos channel to detect active, c-Fos+ neurons. Activity was measured in the c-Fos channel by using the built-in trainable AI image analysis. OPCs somata were reconstructed separately in the PDGFR□ channel (magenta/grey). For every OPC associated within the pyramidal layer of CA1, the distance to the closest active, c-Fos+ neuron was computed in Imaris (distance between 2 surfaces).

e. The distance between OPC somata and c-Fos+ neuronal somata is significantly lower in dcz-injected mice in CA1. Images were taken from 4 mice per group, 5 OPCs per image were measured. Unpaired, two-tailed t-test was performed, t = 3.409, df = 38, p=0.0016.

f. The distance between OPC somata and c-Fos+ neuronal somata is not significantly lower in dcz-injected mice in CA2/3. Images were taken from 4 mice per group, 5 OPCs per image were measuerd. Two-tailed Mann-Whitney test was performed (data not normally distributed), sum of ranks column A: 460; sum of ranks column B: 360; Mann-Whithney U: 150; p=1.1826.

g. vehicle: OPC (magenta) localized in the pyramidal layer of CA1 in between c-Fos+ neurons (green). Spots were seeded onto OPC processes, OPC soma were reconstructed (surface, OPC channel). C-Fos+ neurons were reconstructed (color-coded intensity). 3 Filters were applied to count only spots that are localized on OPC processes within a 4µm range of an active neuronal soma, spots localized on OPC soma were subtracted. Scale bar represents 20µm.

h. dcz-injected mouse: same analysis as in g. Scale bar represents 20µm.

i. Scheme showing how the association of OPC processes with active, c-Fos+ neurons was assessed.

j: in the pyramidal layer of CA1, 14.89% of the spots seeded onto OPC processes were localized within 4 µm around the surface of active neurons in dcz injected mice. This number was significantly lower (9.069%) in vehicle-injected mice. Images were taken from 4 mice per group, unpaired, two-tailed t-test was performed, t = 2.571, df = 6, p=0.0423.

Figure 4. Neurons with contact to OPC processes show lower average calcium transients as compared to those without.

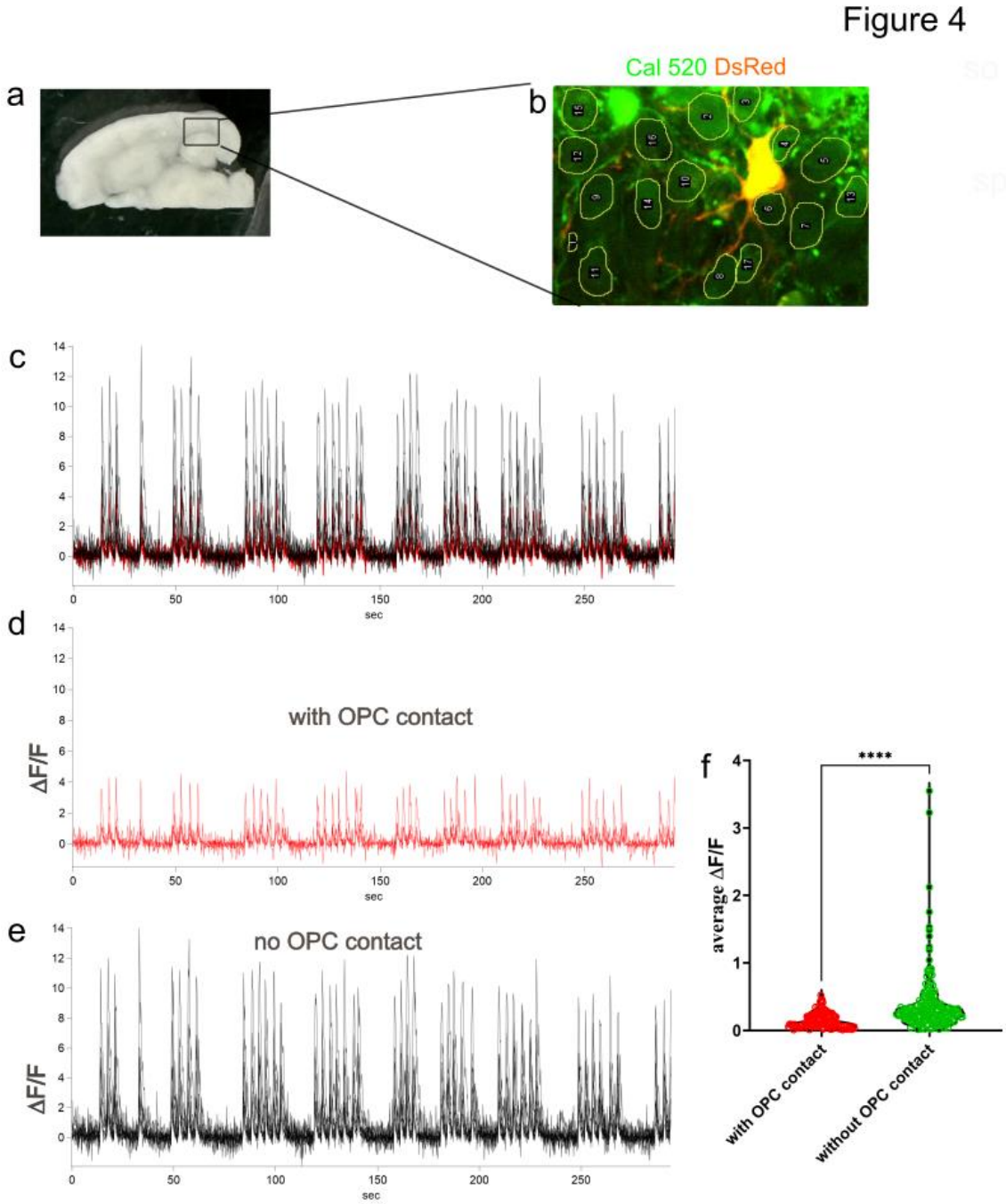

a. acute brain slices were obtained from NG2DsRedBAC transgenic mice at P4.

b. Representative image of the hippocampal pyramidal layer. Neurons were bath-incubated with the Calcium Indicator Cal520 ®. Regions of interest were drawn around neurons next to the OPC (shown in orange) or without OPC contact.

c. Example traces of neurons recorded from the pyramidal layer of the hippocampus.

d. Only traces from neurons with clear OPC contact are shown.

e. Only traces from neurons without OPC contact are shown.

f. Comparison of values for average $\Delta F/F$ are compared between neurons with or without OPC contact. Neurons around 31 different OPCs from 10 mice were analyzed. 114 neurons had close contact to OPCs, 172 were without detectable contact to OPCs. Shapiro-Wilk test was performed to assess normality (<0.0001). Mann-Whitney test was used to compare the 2 groups (p=<0.0001, two-tailed, sum of ranks in column A=10870; B=9273).

Figure 5 Sequencing strategy and bulk RNA-sequencing of P15 hippocampal tissue

Figure 5

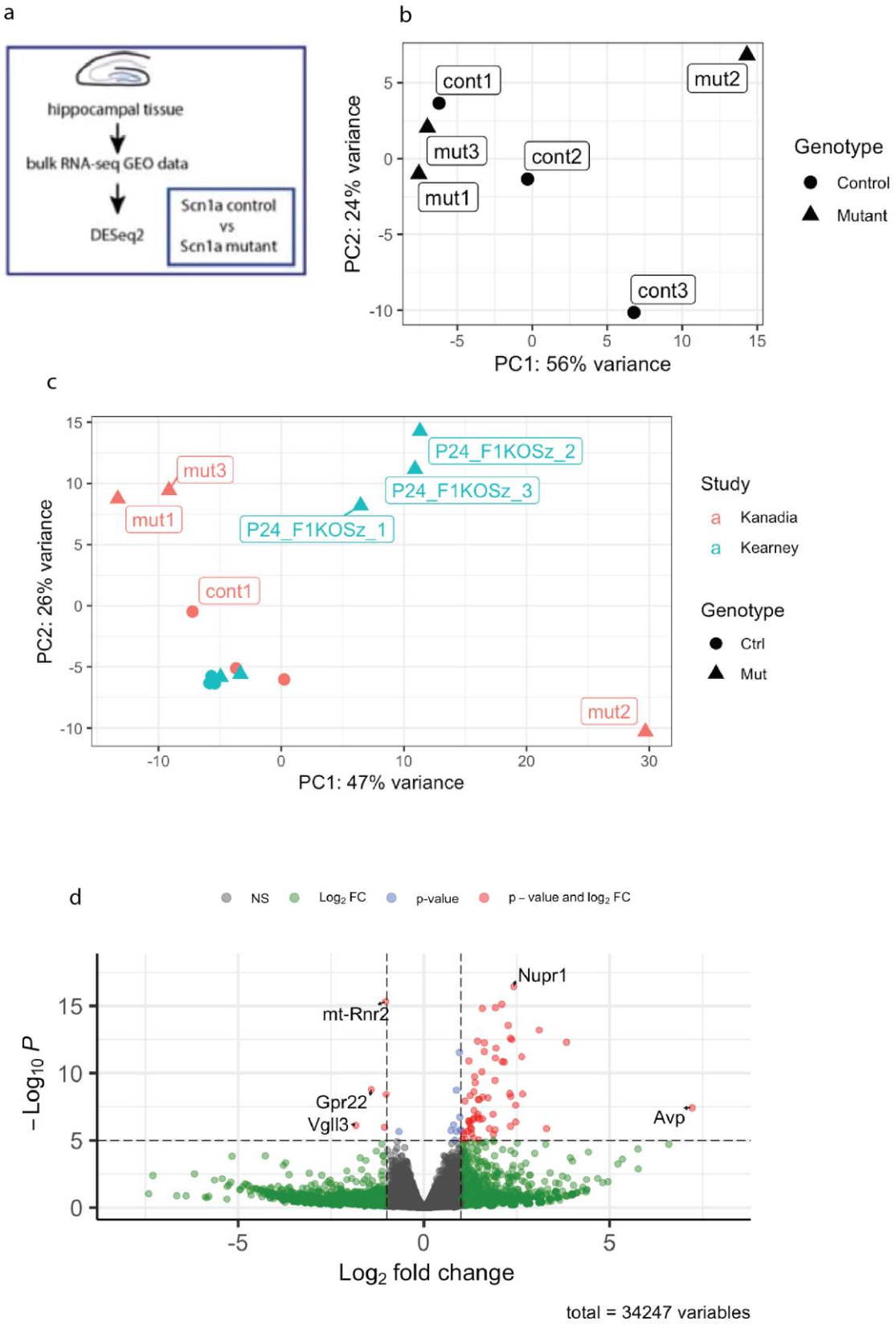

a. Schema showing the experiment for bulk-RNA-seq on hippocampal tissue, using Geo dataset GSE149754.

b. MA plots of all 3 replicates (top; 3 controls, 3 mutants) and only female samples (bottom; 2 controls, 2 mutants), showing $\log_2$FoldChange (y-axis) over the mean counts. Red points indicate genes that were differentially expressed at p-adj < 0.05.

c. Hierarchical clustering of all samples generated by rlog-transformation of normalized counts from DESeq2 analysis. Table shows the sex of the samples.

d. Volcano plot of the outcome of DESeq2 analysis of genes expressed in P15 Scn1a control and mutant hippocampus.

References

Auguste, Y. S. S., Ferro, A., Kahng, J. A., Xavier, A. M., Dixon, J. R., Vrudhula, U., Nichitiu, A. S., Rosado, D., Wee, T. L., Pedmale, U. V., & Cheadle, L. (2022). Publisher Correction: Oligodendrocyte precursor cells engulf synapses during circuit remodeling in mice. *Nat Neurosci*, *25*(12), 1735. https://doi.org/10.1038/s41593-022-01209-z

Badimon, A., Strasburger, H. J., Ayata, P., Chen, X., Nair, A., Ikegami, A., Hwang, P., Chan, A. T., Graves, S. M., Uweru, J. O., Ledderose, C., Kutlu, M. G., Wheeler, M. A., Kahan, A., Ishikawa, M., Wang, Y. C., Loh, Y. E., Jiang, J. X., Surmeier, D. J., . . . Schaefer, A. (2020). Negative feedback control of neuronal activity by microglia. *Nature*, *586*(7829), 417-423. https://doi.org/10.1038/s41586-020-2777-8

Barth, A. L., Gerkin, R. C., & Dean, K. L. (2004). Alteration of neuronal firing properties after in vivo experience in a FosGFP transgenic mouse. *J Neurosci*, *24*(29), 6466-6475. https://doi.org/10.1523/JNEUROSCI.4737-03.2004

Bergles, D. E., & Richardson, W. D. (2015). Oligodendrocyte Development and Plasticity. *Cold Spring Harb Perspect Biol*, *8*(2), a020453. https://doi.org/10.1101/cshperspect.a020453

Bergles, D. E., Roberts, J. D., Somogyi, P., & Jahr, C. E. (2000). Glutamatergic synapses on oligodendrocyte precursor cells in the hippocampus. *Nature*, *405*(6783), 187-191. https://doi.org/10.1038/35012083

Binz, T., Sikorra, S., & Mahrhold, S. (2010). Clostridial neurotoxins: mechanism of SNARE cleavage and outlook on potential substrate specificity reengineering. *Toxins (Basel)*, *2*(4), 665-682. https://doi.org/10.3390/toxins2040665

Brionne, T. C., Tesseur, I., Masliah, E., & Wyss-Coray, T. (2003). Loss of TGF-beta 1 leads to increased neuronal cell death and microgliosis in mouse brain. *Neuron*, *40*(6), 1133-1145. https://doi.org/10.1016/s0896-6273(03)00766-9

Buchanan, J., Elabbady, L., Collman, F., Jorstad, N. L., Bakken, T. E., Ott, C., Glatzer, J., Bleckert, A. A., Bodor, A. L., Brittain, D., Bumbarger, D. J., Mahalingam, G., Seshamani, S., Schneider-Mizell, C., Takeno, M. M., Torres, R., Yin, W., Hodge, R. D., Castro, M., . . . da Costa, N. M. (2022). Oligodendrocyte precursor cells ingest axons in the mouse neocortex. *Proc Natl Acad Sci U S A*, *119*(48), e2202580119. https://doi.org/10.1073/pnas.2202580119

Buenrostro, J. D., Wu, B., Chang, H. Y., & Greenleaf, W. J. (2015). ATAC-seq: A Method for Assaying Chromatin Accessibility Genome-Wide. *Curr Protoc Mol Biol*, *109*, 21 29 21-21 29 29. https://doi.org/10.1002/0471142727.mb2129s109

Butt, A. M., Duncan, A., Hornby, M. F., Kirvell, S. L., Hunter, A., Levine, J. M., & Berry, M. (1999). Cells expressing the NG2 antigen contact nodes of Ranvier in adult CNS white matter. *Glia*, *26*, 84-91.

Cattaruzza, S., Ozerdem, U., Denzel, M., Ranscht, B., Bulian, P., Cavallaro, U., Zanocco, D., Colombatti, A., Stallcup, W. B., & Perris, R. (2013). Multivalent

proteoglycan modulation of FGF mitogenic responses in perivascular cells [Research Support, N.I.H., Extramural

Research Support, Non-U.S. Gov't]. *Angiogenesis*, *16*(2), 309-327. https://doi.org/10.1007/s10456-012-9316-7

Chacon-De-La-Rocha, I., Fryatt, G. L., Rivera, A. D., Restani, L., Caleo, M., Gomez-Nicola, D., & Butt, A. M. (2021). The synaptic blocker botulinum toxin A decreases the density and complexity of oligodendrocyte precursor cells in the adult mouse hippocampus. *J Neurosci Res*, *99*(9), 2216-2227. https://doi.org/10.1002/jnr.24856

Chapman, T. W., Olveda, G. E., Bame, X., Pereira, E., & Hill, R. A. (2023). Oligodendrocyte death initiates synchronous remyelination to restore cortical myelin patterns in mice. *Nat Neurosci*, *26*(4), 555-569. https://doi.org/10.1038/s41593-023-01271-1

Cheli, V. T., Santiago Gonzalez, D. A., Namgyal Lama, T., Spreuer, V., Handley, V., Murphy, G. G., & Paez, P. M. (2016). Conditional Deletion of the L-Type Calcium Channel Cav1.2 in Oligodendrocyte Progenitor Cells Affects Postnatal Myelination in Mice. *J Neurosci*, *36*(42), 10853-10869. https://doi.org/10.1523/JNEUROSCI.1770-16.2016

Chen, P. H., Cai, W. Q., Wang, L. Y., & Deng, Q. Y. (2008). A morphological and electrophysiological study on the postnatal development of oligodendrocyte precursor cells in the rat brain. *Brain Res*, *1243*, 27-37. https://doi.org/10.1016/j.brainres.2008.09.029

Chen, T. J., Kula, B., Nagy, B., Barzan, R., Gall, A., Ehrlich, I., & Kukley, M. (2018). In Vivo Regulation of Oligodendrocyte Precursor Cell Proliferation and Differentiation by the AMPA-Receptor Subunit GluA2. *Cell Rep*, *25*(4), 852-861 e857. https://doi.org/10.1016/j.celrep.2018.09.066

Cheng, J. S., Dubal, D. B., Kim, D. H., Legleiter, J., Cheng, I. H., Yu, G. Q., Tesseur, I., Wyss-Coray, T., Bonaldo, P., & Mucke, L. (2009). Collagen VI protects neurons against Abeta toxicity [Research Support, N.I.H., Extramural

Research Support, Non-U.S. Gov't]. *Nat Neurosci*, *12*(2), 119-121. https://doi.org/10.1038/nn.2240

Chittajallu, R., Aguirre, A., & Gallo, V. (2004). NG2-positive cells in the mouse white and grey matter display distinct physiological properties. *J Physiol*, *561*(Pt 1), 109-122.

Corces, M. R., Trevino, A. E., Hamilton, E. G., Greenside, P. G., Sinnott-Armstrong, N. A., Vesuna, S., Satpathy, A. T., Rubin, A. J., Montine, K. S., Wu, B., Kathiria, A., Cho, S. W., Mumbach, M. R., Carter, A. C., Kasowski, M., Orloff, L. A., Risca, V. I., Kundaje, A., Khavari, P. A., . . . Chang, H. Y. (2017). An improved ATAC-seq protocol reduces background and enables interrogation of frozen tissues. *Nat Methods*, *14*(10), 959-962. https://doi.org/10.1038/nmeth.4396

Cserep, C., Posfai, B., Lenart, N., Fekete, R., Laszlo, Z. I., Lele, Z., Orsolits, B., Molnar, G., Heindl, S., Schwarcz, A. D., Ujvari, K., Kornyei, Z., Toth, K., Szabadits, E., Sperlagh, B., Baranyi, M., Csiba, L., Hortobagyi, T., Magloczky, Z., . . . Denes, A.

(2020). Microglia monitor and protect neuronal function through specialized somatic purinergic junctions. *Science*, *367*(6477), 528-537. https://doi.org/10.1126/science.aax6752

Diniz, L. P., Matias, I., Siqueira, M., Stipursky, J., & Gomes, F. C. A. (2019). Astrocytes and the TGF-beta1 Pathway in the Healthy and Diseased Brain: a Double-Edged Sword. *Mol Neurobiol*, *56*(7), 4653-4679. https://doi.org/10.1007/s12035-018-1396-y

Dityatev, A., & Fellin, T. (2008). Extracellular matrix in plasticity and epileptogenesis. *Neuron Glia Biol*, *4*(3), 235-247. https://doi.org/10.1017/S1740925X09000118

Dobin, A., Davis, C. A., Schlesinger, F., Drenkow, J., Zaleski, C., Jha, S., Batut, P., Chaisson, M., & Gingeras, T. R. (2013). STAR: ultrafast universal RNA-seq aligner. *Bioinformatics*, *29*(1), 15-21. https://doi.org/10.1093/bioinformatics/bts635

Dravet, C., Bureau, M., Dalla Bernardina, B., & Guerrini, R. (2011). Severe myoclonic epilepsy in infancy (Dravet syndrome) 30 years later. *Epilepsia*, *52 Suppl 2*, 1-2. https://doi.org/10.1111/j.1528-1167.2011.02993.x

Fang, L. P., Lin, C. H., Medlej, Y., Zhao, R., Chang, H. F., Guo, Q., Wu, Z., Su, Y., Zhao, N., Gobbo, D., Wyatt, A., Wahl, V., Fiore, F., Tu, S. M., Boehm, U., Huang, W., Bian, S., Agarwal, A., Lauterbach, M. A., . . . Bai, X. (2025). Oligodendrocyte precursor cells facilitate neuronal lysosome release. *Nat Commun*, *16*(1), 1175. https://doi.org/10.1038/s41467-025-56484-8

Favero, M., Sotuyo, N. P., Lopez, E., Kearney, J. A., & Goldberg, E. M. (2018). A Transient Developmental Window of Fast-Spiking Interneuron Dysfunction in a Mouse Model of Dravet Syndrome. *J Neurosci*, *38*(36), 7912-7927. https://doi.org/10.1523/JNEUROSCI.0193-18.2018

Fitzgerald, J. C., Sun, Y., Reinecke, F., Bauer, E., Garaschuk, O., Kahle, P. J., & Pfeiffer, F. (2025). Interactions of Oligodendrocyte Precursor Cells and Dopaminergic Neurons in the Mouse Substantia Nigra. *J Neurochem*, *169*(1), e16298. https://doi.org/10.1111/jnc.16298

Ge, W. P., Yang, X. J., Zhang, Z., Wang, H. K., Shen, W., Deng, Q. D., & Duan, S. (2006). Long-term potentiation of neuron-glia synapses mediated by Ca2+-permeable AMPA receptors. *Science*, *312*(5779), 1533-1537.

Gibson, E. M., Purger, D., Mount, C. W., Goldstein, A. K., Lin, G. L., Wood, L. S., Inema, I., Miller, S. E., Bieri, G., Zuchero, J. B., Barres, B. A., Woo, P. J., Vogel, H., & Monje, M. (2014). Neuronal activity promotes oligodendrogenesis and adaptive myelination in the mammalian brain [Research Support, N.I.H., Extramural

Research Support, Non-U.S. Gov't

Research Support, U.S. Gov't, Non-P.H.S.]. *Science*, *344*(6183), 1252304. https://doi.org/10.1126/science.1252304

Gorski, J. A., Talley, T., Qiu, M., Puelles, L., Rubenstein, J. L., & Jones, K. R. (2002). Cortical excitatory neurons and glia, but not GABAergic neurons, are produced in the

Emx1-expressing lineage. *J Neurosci*, *22*(15), 6309-6314. https://doi.org/10.1523/JNEUROSCI.22-15-06309.2002

Greenberg, M. E., & Ziff, E. B. (1984). Stimulation of 3T3 cells induces transcription of the c-fos proto-oncogene. *Nature*, *311*(5985), 433-438. https://doi.org/10.1038/311433a0

Gregorio, I., Braghetta, P., Bonaldo, P., & Cescon, M. (2018). Collagen VI in healthy and diseased nervous system. *Dis Model Mech*, *11*(6). https://doi.org/10.1242/dmm.032946

Habermacher, C., Angulo, M. C., & Benamer, N. (2019). Glutamate versus GABA in neuron-oligodendroglia communication. *Glia*, *67*(11), 2092-2106. https://doi.org/10.1002/glia.23618

Hawkins, N. A., Calhoun, J. D., Huffman, A. M., & Kearney, J. A. (2019). Gene expression profiling in a mouse model of Dravet syndrome. *Exp Neurol*, *311*, 247-256. https://doi.org/10.1016/j.expneurol.2018.10.010

Hughes, E. G., Kang, S. H., Fukaya, M., & Bergles, D. E. (2013). Oligodendrocyte progenitors balance growth with self-repulsion to achieve homeostasis in the adult brain. *Nat Neurosci*, *16*(6), 668-676. https://doi.org/10.1038/nn.3390

Hughes, E. G., Orthmann-Murphy, J. L., Langseth, A. J., & Bergles, D. E. (2018). Myelin remodeling through experience-dependent oligodendrogenesis in the adult somatosensory cortex. *Nat Neurosci*, *21*(5), 696-706. https://doi.org/10.1038/s41593-018-0121-5

Kirby, L., Jin, J., Cardona, J. G., Smith, M. D., Martin, K. A., Wang, J., Strasburger, H., Herbst, L., Alexis, M., Karnell, J., Davidson, T., Dutta, R., Goverman, J., Bergles, D., & Calabresi, P. A. (2019). Oligodendrocyte precursor cells present antigen and are cytotoxic targets in inflammatory demyelination. *Nat Commun*, *10*(1), 3887. https://doi.org/10.1038/s41467-019-11638-3

Krashes, M. J., Koda, S., Ye, C., Rogan, S. C., Adams, A. C., Cusher, D. S., Maratos-Flier, E., Roth, B. L., & Lowell, B. B. (2011). Rapid, reversible activation of AgRP neurons drives feeding behavior in mice. *J Clin Invest*, *121*(4), 1424-1428. https://doi.org/10.1172/JCI46229

Kukley, M., Capetillo-Zarate, E., & Dietrich, D. (2007). Vesicular glutamate release from axons in white matter. *Nat Neurosci*, *10*(3), 311-320. https://doi.org/10.1038/nn1850

Kuo, F. S., Cleary, C. M., LoTurco, J. J., Chen, X., & Mulkey, D. K. (2019). Disordered breathing in a mouse model of Dravet syndrome. *Elife*, *8*. https://doi.org/10.7554/eLife.43387

Li, Q., Brus-Ramer, M., Martin, J. H., & McDonald, J. W. (2010). Electrical stimulation of the medullary pyramid promotes proliferation and differentiation of oligodendrocyte progenitor cells in the corticospinal tract of the adult rat [Research Support, N.I.H., Extramural

Research Support, Non-U.S. Gov't]. *Neurosci Lett*, *479*(2), 128-133. https://doi.org/10.1016/j.neulet.2010.05.043

Liberzon, A., Birger, C., Thorvaldsdottir, H., Ghandi, M., Mesirov, J. P., & Tamayo, P. (2015). The Molecular Signatures Database (MSigDB) hallmark gene set collection. *Cell Syst*, *1*(6), 417-425. https://doi.org/10.1016/j.cels.2015.12.004

Love, M. I., Huber, W., & Anders, S. (2014). Moderated estimation of fold change and dispersion for RNA-seq data with DESeq2. *Genome Biol*, *15*(12), 550. https://doi.org/10.1186/s13059-014-0550-8

Malone, M., Gary, D., Yang, I. H., Miglioretti, A., Houdayer, T., Thakor, N., & McDonald, J. (2013). Neuronal activity promotes myelination via a cAMP pathway. *Glia*, *61*(6), 843-854. https://doi.org/10.1002/glia.22476

Marques, S., van Bruggen, D., Vanichkina, D. P., Floriddia, E. M., Munguba, H., Varemo, L., Giacomello, S., Falcao, A. M., Meijer, M., Bjorklund, A. K., Hjerling-Leffler, J., Taft, R. J., & Castelo-Branco, G. (2018). Transcriptional Convergence of Oligodendrocyte Lineage Progenitors during Development. *Dev Cell*, *46*(4), 504-517 e507. https://doi.org/10.1016/j.devcel.2018.07.005

Massague, J., Seoane, J., & Wotton, D. (2005). Smad transcription factors. *Genes Dev*, *19*(23), 2783-2810. https://doi.org/10.1101/gad.1350705

McCutcheon, R. A., Reis Marques, T., & Howes, O. D. (2020). Schizophrenia-An Overview. *JAMA Psychiatry*, *77*(2), 201-210. https://doi.org/10.1001/jamapsychiatry.2019.3360

Mercado-Gomez, O., Landgrave-Gomez, J., Arriaga-Avila, V., Nebreda-Corona, A., & Guevara-Guzman, R. (2014). Role of TGF-beta signaling pathway on Tenascin C protein upregulation in a pilocarpine seizure model. *Epilepsy Res*, *108*(10), 1694-1704. https://doi.org/10.1016/j.eplepsyres.2014.09.019

Mickelsen, L. E., Bolisetty, M., Chimileski, B. R., Fujita, A., Beltrami, E. J., Costanzo, J. T., Naparstek, J. R., Robson, P., & Jackson, A. C. (2019). Single-cell transcriptomic analysis of the lateral hypothalamic area reveals molecularly distinct populations of inhibitory and excitatory neurons. *Nat Neurosci*, *22*(4), 642-656. https://doi.org/10.1038/s41593-019-0349-8

Milbrandt, J. (1986). Nerve growth factor rapidly induces c-fos mRNA in PC12 rat pheochromocytoma cells. *Proc Natl Acad Sci U S A*, *83*(13), 4789-4793. https://doi.org/10.1073/pnas.83.13.4789

Morgan, J. I., & Curran, T. (1989). Stimulus-transcription coupling in neurons: role of cellular immediate-early genes. *Trends Neurosci*, *12*(11), 459-462. https://doi.org/10.1016/0166-2236(89)90096-9

Morgan, J. I., & Curran, T. (1991). Stimulus-transcription coupling in the nervous system: involvement of the inducible proto-oncogenes fos and jun. *Annu Rev Neurosci*, *14*, 421-451. https://doi.org/10.1146/annurev.ne.14.030191.002225

Nagy, B., Hovhannisyan, A., Barzan, R., Chen, T. J., & Kukley, M. (2017). Different patterns of neuronal activity trigger distinct responses of oligodendrocyte precursor cells in the corpus callosum. *PLoS Biol*, *15*(8), e2001993. https://doi.org/10.1371/journal.pbio.2001993

Nishiyama, A., Serwanski, D. R., & Pfeiffer, F. (2021). Many roles for oligodendrocyte precursor cells in physiology and pathology. *Neuropathology*. https://doi.org/10.1111/neup.12732

Nishiyama, A., & Stallcup, W. B. (1993). Expression of NG2 proteoglycan causes retention of type VI collagen on the cell surface. *Molecular Biology of the Cell*, *4*, 1097-1108.

Oishi, M., Passlick, S., Yamazaki, Y., Unekawa, M., Adachi, R., Yamada, M., Imayoshi, I., Abe, Y., Steinhauser, C., & Tanaka, K. F. (2023). Separate optogenetic manipulation of Nerve/glial antigen 2 (NG2) glia and mural cells using the NG2 promoter. *Glia*, *71*(2), 317-333. https://doi.org/10.1002/glia.24273

Ong, W. Y., & Levine, J. M. (1999). A light and electron microscopic study of NG2 chondroitin sulfate proteoglycan-positive oligodendrocyte precursor cells in the normal and kainate-lesioned rat hippocampus. *Neuroscience*, *92*, 83-95.

Ortiz, F. C., Habermacher, C., Graciarena, M., Houry, P. Y., Nishiyama, A., Nait Oumesmar, B., & Angulo, M. C. (2019). Neuronal activity in vivo enhances functional myelin repair. *JCI Insight*, *5*. https://doi.org/10.1172/jci.insight.123434

Patel, D. C., Tewari, B. P., Chaunsali, L., & Sontheimer, H. (2019). Neuron-glia interactions in the pathophysiology of epilepsy. *Nat Rev Neurosci*, *20*(5), 282-297. https://doi.org/10.1038/s41583-019-0126-4

Pfeiffer, F., Sherafat, A., & Nishiyama, A. (2021). The Impact of Fixation on the Detection of Oligodendrocyte Precursor Cell Morphology and Vascular Associations. *Cells*, *10*(6). https://doi.org/10.3390/cells10061302

Ramos-Moreno, T., Cifra, A., Litsa, N. L., Melin, E., Ahl, M., Christiansen, S. H., Gotzsche, C. R., Cescon, M., Bonaldo, P., van Loo, K., Borger, V., Jasper, J. A., Becker, A., van Vliet, E. A., Aronica, E., Woldbye, D. P., & Kokaia, M. (2024). Collagen VI: Role in synaptic transmission and seizure-related excitability. *Exp Neurol*, *380*, 114911. https://doi.org/10.1016/j.expneurol.2024.114911

Raudvere, U., Kolberg, L., Kuzmin, I., Arak, T., Adler, P., Peterson, H., & Vilo, J. (2019). g:Profiler: a web server for functional enrichment analysis and conversions of gene lists (2019 update). *Nucleic Acids Res*, *47*(W1), W191-W198. https://doi.org/10.1093/nar/gkz369

Reimand, J., Arak, T., Adler, P., Kolberg, L., Reisberg, S., Peterson, H., & Vilo, J. (2016). g:Profiler-a web server for functional interpretation of gene lists (2016 update). *Nucleic Acids Res*, *44*(W1), W83-89. https://doi.org/10.1093/nar/gkw199

Ricobaraza, A., Mora-Jimenez, L., Puerta, E., Sanchez-Carpintero, R., Mingorance, A., Artieda, J., Nicolas, M. J., Besne, G., Bunuales, M., Gonzalez-Aparicio, M., Sola-

Sevilla, N., Valencia, M., & Hernandez-Alcoceba, R. (2019). Epilepsy and neuropsychiatric comorbidities in mice carrying a recurrent Dravet syndrome SCN1A missense mutation. *Sci Rep*, *9*(1), 14172. https://doi.org/10.1038/s41598-019-50627-w

Serwanski, D. R., Jukkola, P., & Nishiyama, A. (2017). Heterogeneity of astrocyte and NG2 cell insertion at the node of ranvier. *J Comp Neurol*, *525*(3), 535-552. https://doi.org/10.1002/cne.24083

Shannon, P., Markiel, A., Ozier, O., Baliga, N. S., Wang, J. T., Ramage, D., Amin, N., Schwikowski, B., & Ideker, T. (2003). Cytoscape: a software environment for integrated models of biomolecular interaction networks. *Genome Res*, *13*(11), 2498-2504. https://doi.org/10.1101/gr.1239303

Sherafat, A., Pfeiffer, F., Reiss, A. M., Wood, W. M., & Nishiyama, A. (2021). Microglial neuropilin-1 promotes oligodendrocyte expansion during development and remyelination by trans-activating platelet-derived growth factor receptor. *Nat Commun*, *12*(1), 2265. https://doi.org/10.1038/s41467-021-22532-2

Spitzer, S. O., Sitnikov, S., Kamen, Y., Evans, K. A., Kronenberg-Versteeg, D., Dietmann, S., de Faria, O., Jr., Agathou, S., & Karadottir, R. T. (2019). Oligodendrocyte progenitor cells become regionally diverse and heterogeneous with age. *Neuron*, *101*(3), 459-471 e455. https://doi.org/10.1016/j.neuron.2018.12.020

Stallcup, W. B., Dahlin, K., & Healy, P. (1990). Interaction of the NG2 chondroitin sulfate proteoglycan with type VI collagen. *Journal of Cell Biology*, *111*, 3177-3188.

Subramanian, A., Tamayo, P., Mootha, V. K., Mukherjee, S., Ebert, B. L., Gillette, M. A., Paulovich, A., Pomeroy, S. L., Golub, T. R., Lander, E. S., & Mesirov, J. P. (2005). Gene set enrichment analysis: a knowledge-based approach for interpreting genome-wide expression profiles. *Proc Natl Acad Sci U S A*, *102*(43), 15545-15550. https://doi.org/10.1073/pnas.0506580102

Sun, W., Matthews, E. A., Nicolas, V., Schoch, S., & Dietrich, D. (2016). NG2 glial cells integrate synaptic input in global and dendritic calcium signals. *Elife*, *5*. https://doi.org/10.7554/eLife.16262

Susarla, B. T., Laing, E. D., Yu, P., Katagiri, Y., Geller, H. M., & Symes, A. J. (2011). Smad proteins differentially regulate transforming growth factor-beta-mediated induction of chondroitin sulfate proteoglycans. *J Neurochem*, *119*(4), 868-878. https://doi.org/10.1111/j.1471-4159.2011.07470.x

Tarazona, S., Furio-Tari, P., Turra, D., Pietro, A. D., Nueda, M. J., Ferrer, A., & Conesa, A. (2015). Data quality aware analysis of differential expression in RNA-seq with NOISeq R/Bioc package. *Nucleic Acids Res*, *43*(21), e140. https://doi.org/10.1093/nar/gkv711

Thornton, M. A., & Hughes, E. G. (2020). Neuron-oligodendroglia interactions: Activity-dependent regulation of cellular signaling. *Neurosci Lett*, *727*, 134916. https://doi.org/10.1016/j.neulet.2020.134916

Tillet, E., Ruggiero, F., Nishiyama, A., & Stallcup, W. B. (1997). The membrane-spanning proteoglycan NG2 binds to collagens V and VI through the central nonglobular domain of its core protein. *JBC*, *272*, 10769-10776.

Tomassy, G. S., Berger, D. R., Chen, H. H., Kasthuri, N., Hayworth, K. J., Vercelli, A., Seung, H. S., Lichtman, J. W., & Arlotta, P. (2014). Distinct profiles of myelin distribution along single axons of pyramidal neurons in the neocortex [Research Support, N.I.H., Extramural

Research Support, Non-U.S. Gov't]. *Science*, *344*(6181), 319-324. https://doi.org/10.1126/science.1249766

Ulbrich, P., Khoshneviszadeh, M., Jandke, S., Schreiber, S., & Dityatev, A. (2021). Interplay between perivascular and perineuronal extracellular matrix remodelling in neurological and psychiatric diseases. *Eur J Neurosci*, *53*(12), 3811-3830. https://doi.org/10.1111/ejn.14887

Vong, L., Ye, C., Yang, Z., Choi, B., Chua, S., Jr., & Lowell, B. B. (2011). Leptin action on GABAergic neurons prevents obesity and reduces inhibitory tone to POMC neurons. *Neuron*, *71*(1), 142-154. https://doi.org/10.1016/j.neuron.2011.05.028

Wake, H., Ortiz, F. C., Woo, D. H., Lee, P. R., Angulo, M. C., & Fields, R. D. (2015). Nonsynaptic junctions on myelinating glia promote preferential myelination of electrically active axons. *Nat Commun*, *6*, 7844. https://doi.org/10.1038/ncomms8844

Weider, M., Starost, L. J., Groll, K., Kuspert, M., Sock, E., Wedel, M., Frob, F., Schmitt, C., Baroti, T., Hartwig, A. C., Hillgartner, S., Piefke, S., Fadler, T., Ehrlich, M., Ehlert, C., Stehling, M., Albrecht, S., Jabali, A., Scholer, H. R., . . . Wegner, M. (2018). Nfat/calcineurin signaling promotes oligodendrocyte differentiation and myelination by transcription factor network tuning. *Nat Commun*, *9*(1), 899. https://doi.org/10.1038/s41467-018-03336-3

Wennstrom, M., Hellsten, J., Ekdahl, C. T., & Tingstrom, A. (2003). Electroconvulsive seizures induce proliferation of NG2-expressing glial cells in adult rat hippocampus. *Biol Psychiatry*, *54*(10), 1015-1024. https://doi.org/10.1016/s0006-3223(03)00693-0

Wyss-Coray, T. (2006). Tgf-Beta pathway as a potential target in neurodegeneration and Alzheimer's. *Curr Alzheimer Res*, *3*(3), 191-195. https://doi.org/10.2174/156720506777632916

Xiao, Y., Petrucco, L., Hoodless, L. J., Portugues, R., & Czopka, T. (2022). Oligodendrocyte precursor cells sculpt the visual system by regulating axonal remodeling. *Nat Neurosci*, *25*(3), 280-284. https://doi.org/10.1038/s41593-022-01023-7

Yamaguchi, Y., Mann, D. M., & Ruoslahti, E. (1990). Negative regulation of transforming growth factor-beta by the proteoglycan decorin. *Nature*, *346*(6281), 281-284. https://doi.org/10.1038/346281a0

You, W. K., Yotsumoto, F., Sakimura, K., Adams, R. H., & Stallcup, W. B. (2014). NG2 proteoglycan promotes tumor vascularization via integrin-dependent effects on pericyte function [Research Support, N.I.H., Extramural]. *Angiogenesis*, *17*(1), 61-76. https://doi.org/10.1007/s10456-013-9378-1

Yu, G., Su, Y., Guo, C., Yi, C., Yu, B., Chen, H., Cui, Y., Wang, X., Wang, Y., Chen, X., Wang, S., Wang, Q., Chen, X., Hu, X., Mei, F., Verkhratsky, A., Xiao, L., & Niu, J. (2022). Pathological oligodendrocyte precursor cells revealed in human schizophrenic brains and trigger schizophrenia-like behaviors and synaptic defects in genetic animal model. *Mol Psychiatry*, *27*(12), 5154-5166. https://doi.org/10.1038/s41380-022-01777-3

Yu, G., Wang, L. G., Han, Y., & He, Q. Y. (2012). clusterProfiler: an R package for comparing biological themes among gene clusters. *OMICS*, *16*(5), 284-287. https://doi.org/10.1089/omi.2011.0118

Yu, G., Wang, L. G., & He, Q. Y. (2015). ChIPseeker: an R/Bioconductor package for ChIP peak annotation, comparison and visualization. *Bioinformatics*, *31*(14), 2382-2383. https://doi.org/10.1093/bioinformatics/btv145

Zhang, Y., Chen, K., Sloan, S. A., Bennett, M. L., Scholze, A. R., O'Keeffe, S., Phatnani, H. P., Guarnieri, P., Caneda, C., Ruderisch, N., Deng, S., Liddelow, S. A., Zhang, C., Daneman, R., Maniatis, T., Barres, B. A., & Wu, J. Q. (2014). An RNA-sequencing transcriptome and splicing database of glia, neurons, and vascular cells of the cerebral cortex [Research Support, N.I.H., Extramural

Research Support, Non-U.S. Gov't]. *J Neurosci*, *34*(36), 11929-11947. https://doi.org/10.1523/JNEUROSCI.1860-14.2014

Ziskin, J. L., Nishiyama, A., Rubio, M., Fukaya, M., & Bergles, D. E. (2007). Vesicular release of glutamate from unmyelinated axons in white matter. *Nat Neurosci*, *10*(3), 321-330. https://doi.org/10.1038/nn1854